Europe
European Chemical
Societies Publishing

▌**Perylene Monoimide Dyes** |*Hot Paper*|

1,7,9,10-Tetrasubstituted PMIs Accessible through Decarboxylative Bromination: Synthesis, Characterization, Photophysical Studies, and Hydrogen Evolution Catalysis

Daniel Costabel,[a] Artem Skabeev,[a] Afshin Nabiyan,[a] Yusen Luo,[b] Johannes B. Max,[a] Ashwene Rajagopal,[c] Daniel Kowalczyk,[d] Benjamin Dietzek,[b, e, f] Maria Wächtler,[b, e] Helmar Görls,[g] Dirk Ziegenbalg,[d] Yulian Zagranyarski,[h] Carsten Streb,[c] Felix H. Schacher,[a, f] and Kalina Peneva*[a, f]

Abstract: In this work, we present a new synthetic strategy for fourfold-substituted perylene monoimides via tetrabrominated perylene monoanhydrides. X-ray diffraction analysis unveiled the intramolecular stacking orientation between the substituents and semicircular packing behavior. We observed the remarkable influence of the substituent on the longevity and nature of the excited state upon visible light excitation. In the presence of poly(dehydroalanine)-graft-poly(ethylene glycol) graft copolymers as solubilizing template, the chromophores are capable of sensitizing $[Mo_3S_{13}]^{2-}$ clusters in aqueous solution for stable visible light driven hydrogen evolution over three days.

Introduction

Organic photoactive materials are promising candidates for molecular artificial photosynthetic systems because of their low cost, earth abundance, and the chemical tunability of their properties well-established synthetic procedures; however, to date, most of these systems lack sufficient photostability.[1] Amongst photoactive materials, perylene-based chromophores have received major interest due to their excellent visible light absorption, photostability and earth abundant composition. Furthermore, the different positions of the perylene framework can be selectively addressed to tune the electrochemical and photophysical properties so that they can match various cata-

lysts or semiconductor materials.[2,3] These properties lead to a variety of applications in the field of organic electronics like organic photovoltaics,[4–9] photocatalysis,[10–16] organic field effect transistors[17–19] as well as biomedical applications.[20–24] Perylene monoimides (PMIs) and perylene diimides (PDI) possess several positions that are easily accessible for further chemical modification and therefore provide a convenient way to further fine tune the stability and photophysical properties of the chromophore. The vast majority of perylenes applied so far as photosensitizers are PDIs, which are rather electron poor and this limits their application mainly electron acceptors.[11,14,25–26] Nevertheless, there is a large demand of stable photosensitizers based on electron-rich organic molecules. The introduction of

[a] D. Costabel, A. Skabeev, A. Nabiyan, J. B. Max, Prof. Dr. F. H. Schacher, Prof. Dr. K. Peneva
Institute of Organic Chemistry and Macromolecular Chemistry
Friedrich Schiller University Jena
Lessingstraße 8, 07743 Jena (Germany)
E-mail: Kalina.Peneva@uni-jena.de

[b] Dr. Y. Luo, Prof. Dr. B. Dietzek, Dr. M. Wächtler
Institute of Physical Chemistry and Abbe Center of Photonics
Friedrich Schiller University Jena
Helmholtzweg 4, 07743 Jena (Germany)

[c] Dr. A. Rajagopal, Prof. Dr. C. Streb
Institute of Inorganic Chemistry 1, Ulm University
Albert-Einstein-Allee 11, 89081 Ulm (Germany)

[d] D. Kowalczyk, Prof. Dr. D. Ziegenbalg
Institute of Chemical Engineering, Ulm University
Albert-Einstein-Allee 11, 89081 Ulm (Germany)

[e] Prof. Dr. B. Dietzek, Dr. M. Wächtler
Department of Functional Interfaces
Leibniz Institute of Photonic Technology Jena
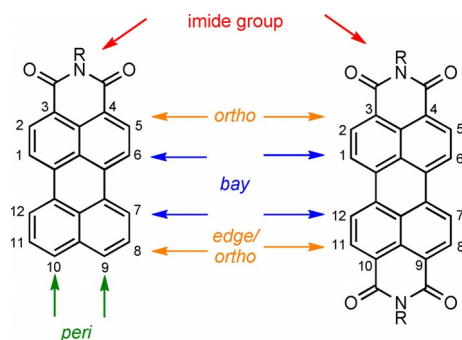Albert-Einstein-Straße 9, 07745 Jena (Germany)

[f] Prof. Dr. B. Dietzek, Prof. Dr. F. H. Schacher, Prof. Dr. K. Peneva
Center for Energy and Environmental Chemistry Jena and
Jena Center of Soft Matter, Friedrich Schiller University Jena
Philosophenweg 7a, 07743 Jena (Germany)

[g] Dr. H. Görls
Institute of Inorganic and Analytical Chemistry
Friedrich Schiller University Jena
Humboldt Straße 8, 07743 Jena (Germany)

[h] Assoc. Prof. Dr. Y. Zagranyarski
Faculty of Chemistry and Pharmacy
Sofia University "St. Kliment Ohridski"
1 James Bourchier Blvd., 1164 Sofia (Bulgaria)

☐ Supporting information and the ORCID identification numbers for the authors of this article can be found under:
https://doi.org/10.1002/chem.202004326.

Chemistry–A European Journal

Full Paper
doi.org/10.1002/chem.202004326

Chemistry Europe
European Chemical
Societies Publishing

Figure 1. Chemical structure of perylene monoimide (left) and perylene di-imide (right) and their different positions.

halogen atoms as substituents in the *bay* region has proven to be one of the most versatile methods for chemical modification of the rylene scaffold and has resulted in a myriad of substituted rylene mono- and diimides (Figure 1). Müllen and co-workers showed that the substitution of 1,6,9-tribromopery-lene 3,4-monoimide with electron-donating groups establishes "push–pull" chromophores with narrow band gaps below 1 eV.[27–28] The brominated building blocks are not only applied in nucleophilic aromatic substitution and studies of substitution patterns,[29] but they also allow the application of palladium-catalyzed cross-coupling reactions such as Suzuki,[30–31] Sonogashira[32–33] or Buchwald–Hartwig cross-coupling.[34–35] Valiyaveettil and co-worker later reported bromination of PMIs resulting in mixtures of tribromo PMIs (81% yield) and 1,6,9,10-tetrabromo PMI (13% yield) which underwent subsequent Suzuki coupling.[36] Koner et al. adopted the idea of using multiple brominated perylene monoimides (PMI) to introduce different electron-donating groups to the perylene scaffold by synthesizing 1,6,9,10-tetrabromo PMI with 46% yield followed by nucleophilic aromatic substitutions with different substituted phenols and thiophenols.[37,38] Although many of these earlier works have demonstrated the potential of the rylene scaffold, some of the procedures use up to 200 equivalents of bromine during the synthesis which could effectively prevent any possible large-scale applications. Therefore, in the search for novel photoactive materials, the discovery of straightforward synthetic procedures that give the desired photosensitizers in high yields and use more environmentally friendly procedures is essential to be able to create safe and ecofriendly alternatives to fossil fuels.

We report herein the synthesis of 1,6,9,10- and 1,7,9,10-tetra-bromoperylene 3,4-dibutyl ester accomplished in three steps from perylene 3,4,9,10-dianhydride with a total bromine excess of only sevenfold, excellent control over the substitution pattern by the first bromination step and an overall yield of more than 55%. We used the decarboxylative bromination Huns-diecker reaction, previously applied to different perylene dia-nhydrides (PDA)[39–41] on either 1,6-dibromo PDA, 1,7-dibromo PDA or isomeric mixtures. These compounds were esterified to enhance the solubility and separate the two isomers (**3a** and **3b**).[42] Subsequently, different substituents like phenoxy (**4**), thiophenoxy (**5** and **5b**) and selenophenoxy (**6**) were intro-

duced in excellent yields (60–99%) and the resulting dyes were converted by acidic hydrolysis and imidization to pery-lene monoimides (**10**–**12**). UV/Vis absorption spectroscopy, fluorescence spectroscopy (emission, lifetime, quantum yield) and cyclic voltammetry have been employed to investigate the electronic and photophysical properties of the new chromophores. Furthermore, single crystals were obtained for the PDEs and their structures were determined by single crystal X-ray diffraction. Photocatalytic hydrogen evolution tests were carried out in a custom-made, 3D printed photoreactor with $(NH_4)_2[Mo_3S_{13}]$ to determine the activity of the new dyes as photosensitizers. The used photoreactor standardized reaction conditions during the photocatalytic experiments and allowed control over the used light source. Transient absorption spectroscopy was furthermore applied to gain insights to the excited states and their relaxation pathways.
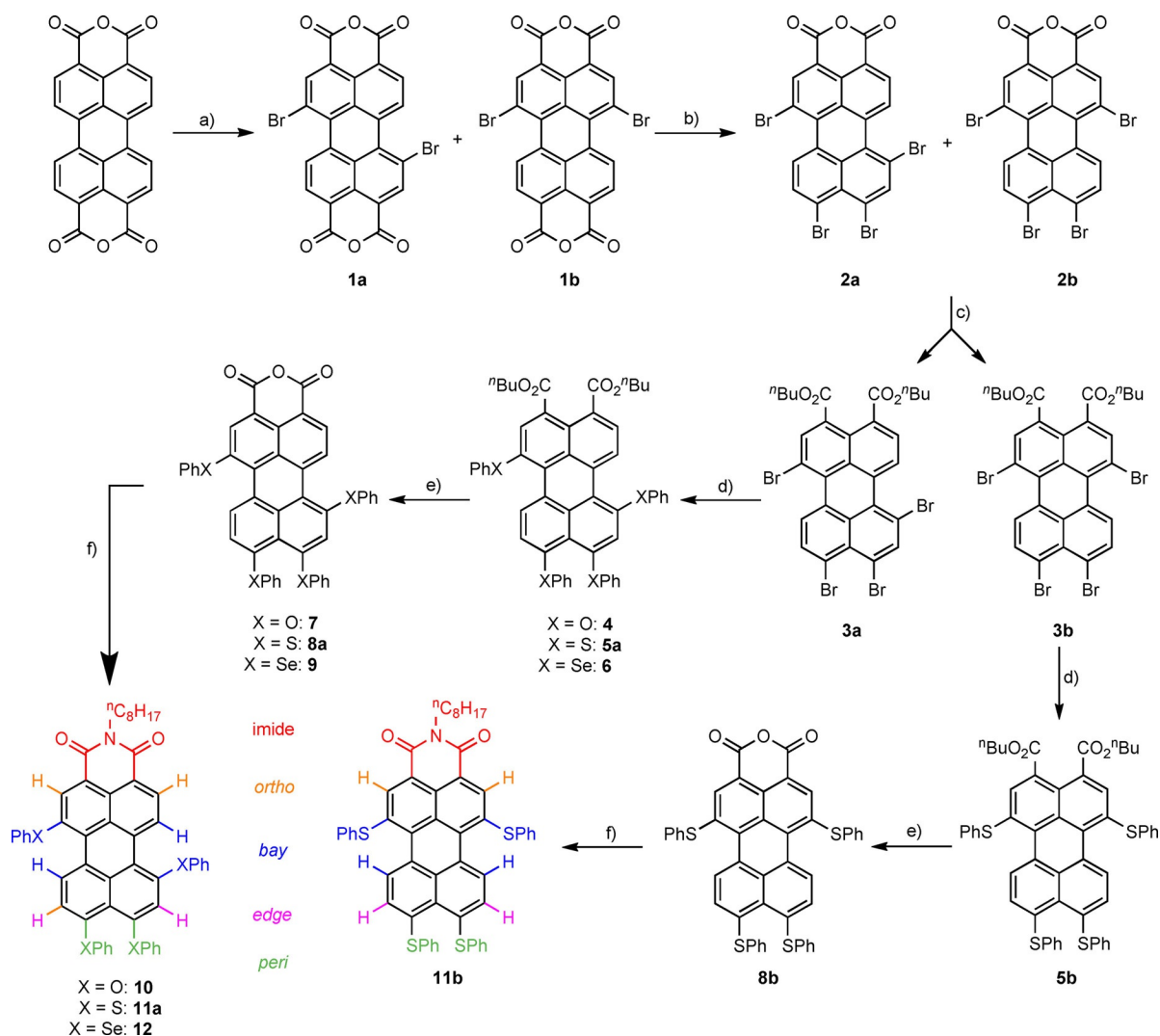
Results and Discussion

Synthesis

Initially, perylene dianhydride (PDA) was brominated in sulfuric acid and bromine in the presence of catalytic amounts of iodine. As described earlier, this reaction led to a major product 1,7-dibromo PDA ($\approx 80\%$, **1a**) and 1,6-dibromo PDA as side product ($\approx 20\%$, **1b**; Figure 2).[43] In the following step, the introduction of two bromo-substituents in the *peri* positions 9 and 10 was performed as in the previously reported procedure with the addition of tetrabutylammonium hydroxide.[39,44] Following esterification, the corresponding perylene dibutyl esters (**3a** and **3b**) were obtained. Column chromatography was used to separate 1,7,9,10-tetrabromo PDE **3a** from 1,6,9,10-tetrabromo PDE **3b**, where the two chromophores were isolated in 45 and 11% yield, respectively, over three steps. Tetrabromo-substituted PMI derivatives have been previously described, however, the method described here gives access to 1,6,9,10- and 1,7,9,10-isomers in high isomeric purity and it uses a modest sevenfold excess of bromine combined for both bromination steps.[37] Subsequently, we introduced four phenoxy- (**4**, 75%), thiophenoxy- (**5a**; **5b**, 99%) or seleno-phenoxy-substituents (**6**, 60%) in DMF with Cs_2CO_3 starting from the respective dibutyl esters (**3a**; **3b**). A further modification addressed the carboxy-groups of the perylene scaffold. Acidic hydrolysis of the ester moieties led to the corresponding PMAs **7**–**9** (76–82%). Next, N-octyl PMIs (**10**–**12**, 84–87%) were synthesized from the different PMAs by imidizations in NMP with different amounts of acetic acid. The chemical structure of all novel compounds was identified by NMR spectroscopy (^1H NMR, $^{13}C\{^1H\}$ NMR, $^{77}Se\{^1H\}$ NMR, $^1H,^1H$ COSY NMR), as well as mass spectrometry (HR-APCI neg.).

Single-crystal X-ray diffraction

In addition, the diffusion of *n*-hexane into dichloromethane solutions of compounds **3a**, **3b**, **4**, **5** and **6** led to the formation of single crystals suitable for X-ray diffraction studies, shown in Figure 3. The average torsion between the two naph-
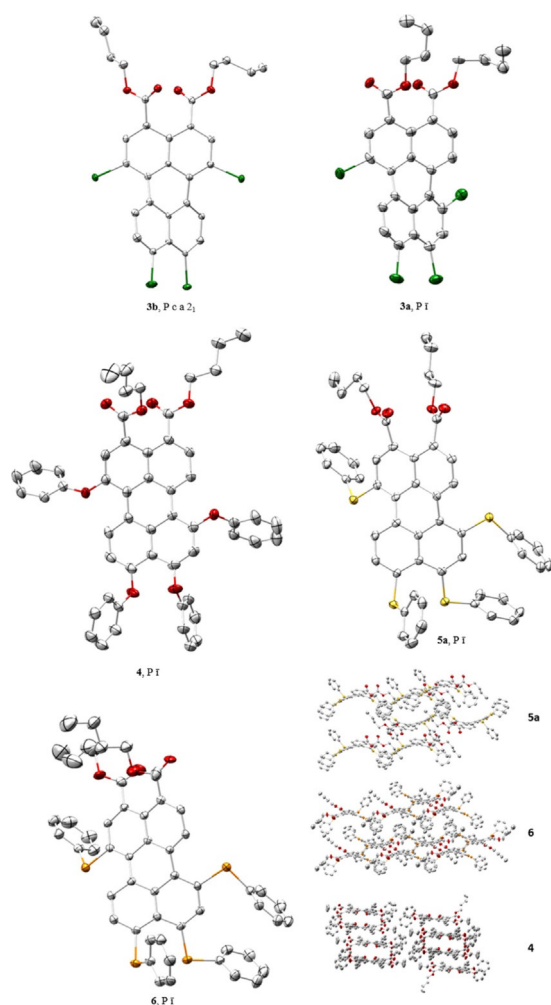
Chemistry–A European Journal

Full Paper
doi.org/10.1002/chem.202004326

Chemistry Europe
European Chemical
Societies Publishing

Figure 2. Synthetic procedure for PDEs **3a–6**, PMAs **7–9** and PMIs **10–12**. a) i: H_2SO_4, 55 °C, 30 h; ii: I_2, 5 h; iii: Br_2, 85 °C, 24 h; b) i: KOH, H_2O, THF, 60 °C, 1 h; ii: nBu_4NOH, 1 h; iii: Br_2, 3 h; c) i: $nBuOH$, DBU, DMF, 80 °C, 1 h; ii: $nBuBr$, 4 h; d) HXPh, Cs_2CO_3, DMF, 100 °C, 14 h; e) pTsOH·H_2O, toluene, 100 °C, 30 h; f) H_2N-C_8H_{17}, 150 °C, 15–60 min.

thalene units was determined at 28.9(12)° for **3a** and 27.7(14)° for **3b**, which is a result of the repulsion of the bromo substituents in the bay region compared to the respective protons. This 1–4 strain also causes the Br-C—C angles deviation from its natural 120° (**3a**: 124.0(6)°; **3b**: 124.4(7)°). The structure of **4** (Figure 3) however, showed a slightly disturbed packing of the butyl ester in position 4 of the perylene framework and a smaller torsion (19.2(12)°) due to the smaller van der Waals radius of oxygen compared to bromine. The torsion of the perylene framework was found with 27.5(12)° (**5a**, Figure 3) and 26.6(14)° (**6**, Figure 3). The smaller torsion for **6** compared to **5** is attributed to the enhanced van der Waals radius (**5a**: 1.8(3) Å, **6**: 1.9(4) Å) and less 1–4 strain. A noticeable observation is the orientation of aryl substituents in positions 7 and 9 of the chromophore. For **5a** and **6**, the phenyl rings face each other with centroid–centroid distances of 3.80 and 3.82 Å, respectively, which are within the reported range of π–π interactions.[45] As a result, the angle alongside the heteroatom phenyl axis deviates from 180° by a margin of 6.9°

(**5a**) and 9.4° (**6**), respectively. However, this behavior was not observed for compound **4**. The structures of **5a** and **6** display ball-shaped overlapping of both the substituents and the distorted perylene framework while the packing behavior for **4** was found to be squared. The molecular packing behavior can play a major role in self-assembled photocatalytic systems. Stupp and co-workers reported that the crystalline packing behavior of PMI-based photosensitizers can have an important contribution to the photocatalytic performance in hydrogels.[46–48]
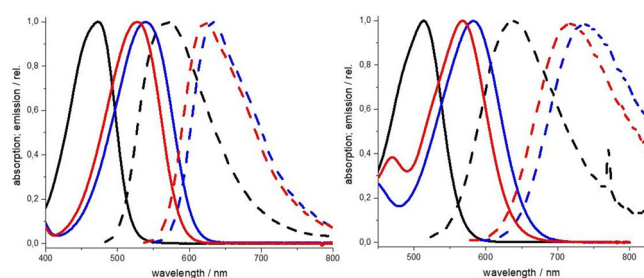
Spectroscopy

We investigated the optical properties of all compounds to get an insight on the electron-donating influence of the different substituents and the electron-withdrawing strength of the dibutyl ester, monoanhydride, and N-octylimide moieties to the chromophore. All measurements were carried out in dichloromethane at 25 °C. Compared to **3a** with $\lambda_{abs,max}$ 471 nm, com-

Chemistry–A European Journal

Full Paper
doi.org/10.1002/chem.202004326

**Chemistry
Europe**
European Chemical
Societies Publishing

Figure 4. Absorption (solid) and emission (dashed) spectra in CH$_2$Cl$_2$. Left: compounds **4** (black), **7** (blue) and **10** (red); right: compounds **5 a** (black), **8 a** (blue) and **11 a** (red).

Figure 3. Molecular structures of compound **3 a** (top right), **3 b** (top left), **4** (middle left), **5 a** (middle right), **6** (bottom left) and packing of **4**, **5 a**, **6** (bottom right); bottom right), 60 % probability, hydrogen atoms are omitted for clarity.

pounds **5** and **6** show a bathochromic shift in $\lambda_{abs,max}$ by 39 and 43 nm, respectively. In contrast, the difference in the absorption maximum of **3 a** and **4** is at a negligible value of 1 nm. The differences in the substitution pattern showed almost no influence on the absorption maxima (**3 a**: 471 nm, **3 b**: 474 nm; **5**: 513 nm, **5 b**: 514 nm). The corresponding perylene monoanhydrides **7**–**9** show bathochromic shifts in $\lambda_{abs,max}$ of 64 to 69 nm compared to their respective PDEs while PMIs **10**–**12** have a hypsochromic shift of 12 to 16 nm in their $\lambda_{abs,max}$, compared to the corresponding PMAs. Emission of tetrabromo PDEs showed Stokes shift of 37 (**3 a**) and 47 nm (**3 b**), respectively, whereas phenoxy-, thiophenoxy- and selenophenoxy- substituted PDEs **4**–**6** had shifts between 100 and 123 nm. Thiophenoxy-substituted PMA **8 a**, **8 b** and PMI **11 b** had the biggest bathochromically shifted $\lambda_{em,max}$ at 737, 753 nm and 725 nm with shifts of 155 to 172 nm as a result of the strong push-pull effect alongside the chromophore axis. In contrast, PMA **7** and PMI **10** showed distinctively smaller Stokes shifts between 91 and 95 nm due to the weaker electron donation ability of the phenoxy substituents. The influ-

ence of the ester, anhydride and imide moiety on absorption and emission are displayed exemplarily in Figure 4 for the phenoxy substituted compounds **4**, **7** and **10** (left) as well as for thiophenoxy substituted compounds **5 a**, **8 a** and **11 a** (right). Perylene diester, anhydrides and monoimides are known for their very high fluorescence quantum yields and compounds **3 a** and **3 b**, **4**, **7** and **10** are no exception to that.[49] Quantum yields ranging between 48 and 88 % were observed. At the same time, the presence of strongly electron-donating groups often leads to significant reduction of the emissive relaxation pathways.[37,50] Li and co-workers observed, that a certain geometry of the electron-donating groups towards the acceptor perylene monoimide framework favors spin-orbit charge transfer intersystem crossing (SOCT-ISC).[51,52] This can explain the decrease in fluorescence quantum yield for compounds **5**(**a** and **b**), **6**, **8**(**a** and **b**), **9** and **11**(**a** and **b**), **12** which did not display quantum yields above 4 %. In fact, the presence of thiophenoxy or selenophenoxy substituents at the chromophore quenched the emission for compounds **5**(**a** and **b**), **6**, **8**(**a** and **b**), **9** and **11 b** to below 1 %. For compounds **3**(**a** and **b**), **4**, **7** and **10**, lifetimes between 4.0 and 5.8 ns were obtained in dichloromethane, which is in the reported range of comparable perylene based dyes.[29,37] Due to the poor fluorescence quantum yields of thiophenoxy- and selenophenoxy-substituted compounds, emission lifetime could not be determined.
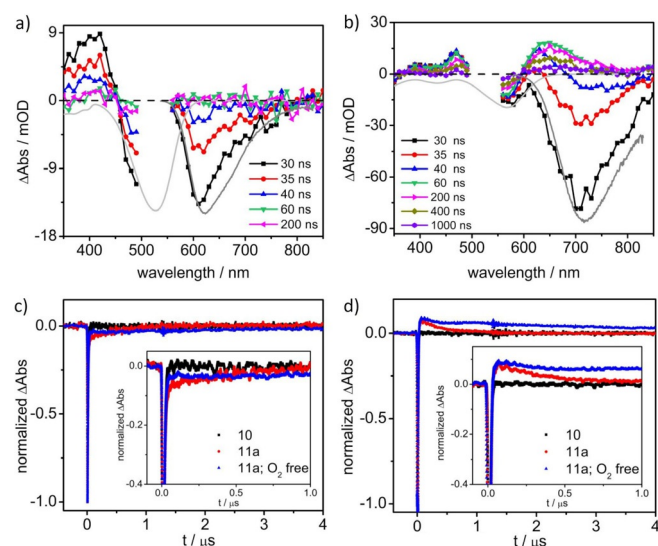
Electrochemistry

Reduction and oxidation potentials of the dyes were investigated using cyclic voltammetry. The redox potentials were designated against the Fc/Fc$^+$ couple and thereof, the energetic positions of the frontier molecular orbitals were calculated. The cyclic voltammogram of **3 a** showed a reversible oxidation process at 1.08 V (halfwave) representing the formation of a radical cation. Three reduction processes were observed in the cathodic direction at -1.6, -1.7, and -1.8 V (peak potentials), which shows a wide shift to more negative potentials when compared to 1,7-dibromoperylene tetrabutyl ester. In contrast to the latter compound, the reduction processes were not found to be reversible in the anodic sweep.[42] This indicates reductive degradation of the compound which was found exclusively for **3**(**a** and **b**) implying that this process is strongly related to the bromo substituents. PDEs **4** to **6** show their first oxi-

dation value at lower potentials (0.44, 0.47, 0.52 V) and **5**(**a** and **b**) and **6** have their first reduction event at −1.66 and −1.68 V respectively. In contrast, the reduction of **4** −1.87 V and its estimated LUMO is at −2.93 eV displaying both a higher LUMO and a bigger band gap compared to **5**(**a** and **b**) and **6** which is in agreement with the minor electron donation in compound **4**. As expected, due to the electron withdrawing nature of the anhydride, the first reduction events of PMAs **7**–**9** are observed at considerably less negative potentials, compared to their respective PDEs. Additionally, PMA **8 a** showed the lowest electrochemical band gap with 1.85 eV which illustrates the desired push-pull behavior. PMIs **10** and **11**(**a** and **b**) expressed a comparable electrochemical behavior. Unlike in the literature, **10** displayed redox potentials in the range of reported 1,6,9,10-tetra(4-*tert*-octylphenoxy) PMI, while the first reduction event of **11 a** at −1.38 V was shifted by 0.48 V to more negative potential compared to its reported 1,6-derivative (−0.9 V). A proportionate shift to lower potentials was observed for the oxidation of **11 a**.[37]

Transient absorption spectroscopy

Nanosecond transient absorption (TA) spectroscopy was performed to investigate the PMI photosensitizers' excited state. Figure 5 exemplarily shows the ns TA spectra of **10** and **11 a** upon excitation at 525 nm in aerated CH$_2$Cl$_2$ (for **11 b** and **12**, see Figures S21 and S23). At 30 ns, the TA spectrum displays the characteristics of the singlet PMI excited-state:[51,52] a positive differential absorption band below 450 (for **10**, Figure 5 a) or 500 nm (for **11 a**, Figure 5 b), a negative band at the position of the ground-state absorption, and a strong negative feature above 550 (for **10**, Figure 5 a) or 600 nm (for **11 a**, Figure 5 b)

associated with residual emission assigned by a comparison with the steady state emission spectra and additional measurements at the ns transient absorption setup only detecting emission (Figure S18c). However, the evolution of the ns TA spectra for **11 a** qualitatively differs from **10**. For **10**, the ns TA spectra have decayed entirely within the first 60 ns (Figure 5 a), while for **11 a**, the decay involves two distinct processes: between 30 and 60 ns the negative, emission associated band at 700 nm decays, while a positive differential absorption at 650 nm appears. Afterwards, the ns TA features decay without further spectral changes on a sub-microsecond timescale. **11 b** and **12** (Figure S21 and S23) behave similarly to **11 a**. This observation points to a long-lived state being formed after photoexcitation of the thiophenoxy or selenophenoxy substituted PMI chromophores, which is not present in **10**.

A global fit of the ns TA data of **10** yields a monoexponential decay with a short-lived component, $\tau_{ns1} < 10$ ns in agreement with the fluorescence lifetime determined in the streak camera measurements of 4.8 ns (Table 1). The associated short-lived state is emissive (Figure S18c) and its emission resembles the spectral shape of the steady-state fluorescence. Thus, it represents the decay of the singlet excited state. For **11 a** (and also for **11 b** and **12**, see Figures S21b and S23b), a global fit yields a biexponential decay (Table 2) with a short-lived emissive component ($\tau_{ns1} < 10$ ns, Figure S19b) and a longer-lived nonemissive component ($\tau_{ns2} = 350$ ns, Figure S19b). The sub-10 ns component is again attributed to the decay of the singlet excited state in **11 a**. However, a larger fraction of the excited molecules populates a long-lived dark state, which decays back to the ground state with τ_{ns2}. Furthermore, it is found that the lifetime of the τ_{ns2} component depends strongly on the concentration of oxygen in solution: $\tau_{ns2} = 350$ ns in aerated CH$_2$Cl$_2$ versus $\tau_{ns2} = 4500$ ns in deaerated CH$_2$Cl$_2$ (Figures 5 c, d and S20; for **11 b** and **12** see Figures S21–24). The significantly increased lifetime in the absence of oxygen points

Figure 5. Nanosecond transient absorption spectra of a) **10** and b) **11 a** collected after excitation at 525 nm in aerated CH$_2$Cl$_2$. The light and dark gray lines represent the shapes of the corresponding inverted ground-state absorption and emission spectrum, respectively. The two steady-state spectra were arbitrarily scaled to fit the respective figure. Comparison of the normalized kinetics at c) 580 and d) 650 nm. Insets: enlargements of the time region up to 1 µs.

Table 1. Absorbance, emission, and redox properties.

	λ_{max} [nm][a]	ε [M^{-1}cm^{-1}]	λ_{em} [nm][a]	Φ_{em} [%][a]	τ [ns][a]	E_{red1} [V][b]	E_{ox1} [V][b]	E_{LUMO} [eV][c]	E_{HOMO} [eV][c]
3 a	471	27 681	508	48	5.8	−1.44**	1.08	−3.36	−5.88
3 b	474	24 082	521	74	4.0	−1.40**	1.10	−3.40	−5.90
4	472	8 607	572	88	4.9	−1.87	0.44	−2.93	−5.24
5 a	513	23 570	637	1	*	−1.66	0.47	−3.14	−5.27
5 b	514	21 961	634	0	*	−1.66	0.48	−3.14	−5.28
6	510	28 124	623	1	*	−1.68	0.52	−3.12	−5.32
7	539	28 452	630	73	5.8	−1.55	0.50	−3.25	−5.30
8 a	582	18 643	737	1	*	−1.24	0.61	−3.56	−5.41
8 b	581	33 232	753	0	*	−1.22	0.62	−3.58	−5.42
9	578	28 592	706	0	*	−1.25	0.62	−3.55	−5.42
10	527	28 950	622	67	4.8	−1.40	0.59	−3.40	−5.39
11 a	568	28 866	716	3	*	−1.38	0.53	−3.42	−5.33
11 b	567	29 406	723	0	*	−1.36	0.55	−3.44	−5.35
12	564	30 870	686	4	*	−1.40	0.57	−3.40	−5.37

[a] In CH$_2$Cl$_2$. [b] Redox potentials (half wave) measured by cyclic voltammetry in CH$_2$Cl$_2$-[(*n*Bu$_4$N)(PF$_6$)] at 0.2 V s^{-1} against the Fc/Fc$^+$ couple. [c] Frontier molecular orbital values are given in eV and estimated by $E_{LUMO} = -(4.8\ eV + E_{Red1})$ and $E_{HOMO} = -(4.8\ eV + E_{Ox1})$. *Not detectable due to poor emission quantum yield. **Peak potential due to irreversibility.

Chemistry–A European Journal

Full Paper
doi.org/10.1002/chem.202004326

**Chemistry Europe**
European Chemical
Societies Publishing

Table 2. Global fit results of the nanosecond transient absorption data in aerated and deaerated dichloromethane. τ_{ns1} is within the time resolution of the setup (~ 10 ns).

	Aerated CH_2Cl_2 τ_{ns1} [ns]	τ_{ns2} [ns]	Deaerated CH_2Cl_2 τ_{ns1} [ns]	τ_{ns2} [ns]
10	< 10	–	–	–
11a	< 10	350	< 10	4500
11b	< 10	300	< 10	6500
12	< 10	320	< 10	1100

to the nature of a triplet state (τ_{ns2} component). Hence, upon excitation there is a long-lived triplet state formed in **11a** (also in **11b** and **12**) while in **10** the initially excited singlet excited state decays completely to the ground state with a time constant < 10 ns. This observation is also in line with the observed fluorescence emission quantum yields that **10** displays a relative quantum yield of 67% while for **11a** the fluorescence emission is only 3% (Table 1).
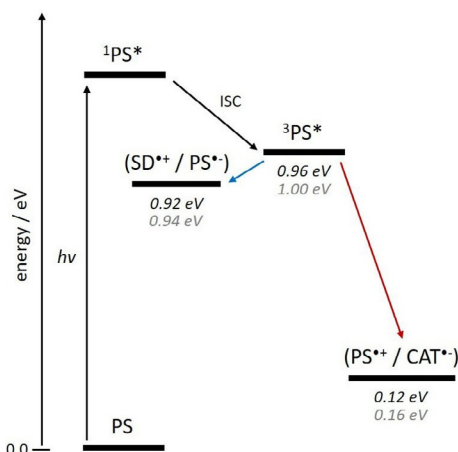
Light-driven hydrogen evolution catalysis

Long-lived excited states have proven to be beneficial to photo-induced electron transfer since they prolong the timeframe of possible charge transfer.[55] Perylene monoimides **10–12** were investigated as photosensitizers with $(NH_4)_2[Mo_3S_{13}]\cdot2H_2O$ as a hydrogen evolution catalyst. Molecular molybdenum sulfide clusters have been extensively studied for light-driven hydrogen evolution and have shown high catalytic efficiency in combination with several photoactive light absorbers (Table S1),[56–60] amongst them a broad scope of perylene-based chromophores.[47, 58, 59] An efficient light-driven reaction involving hydrophobic photosensitizers like the perylene dyes reported here requires the addition of a solubilizing agent. In our case, we chose a poly(dehydroalanine)-*graft*-poly(ethylene glycol) graft copolymer (PDha-*g*-PEG), as this exhibits a charged backbone, broad solubility in water over the entire pH range and has been shown to solubilize both hydrophobic carbon nanotubes as well as to serve as template for the formation of AgAu alloy nanoparticles.[61, 62] Additionally, the presence of a water-soluble polymeric surfactant has also shown to stabilize the catalyst. For that purpose, PMI **10–12** were dispersed in aqueous solution containing PDha-*g*-PEG. After mixing, dynamic light scattering (DLS) indicated the formation of aggregates with a hydrodynamic radius of about 15 nm (DLS, Figure 6f) which could be confirmed by transmission electron microscopy (TEM, Figure 6c). We were also interested in the morphology of the formed nanohybrids and, according to TEM, spherical objects with an average diameter of 50 nm in the dried state were found (Figure 6c) for PDha-*g*-PEG/**12** dispersion. In light-driven hydrogen evolution experiments (a detailed description is given in the Supporting Information), catalytic hydrogen production was observed with compounds **11a** and **12** as photosensitizers (Figure 7). No hydrogen production was observed without catalyst, sacrificial electron donor, photosensitizer, graft copolymer or irradiation (Table 3). With thiophenoxy substituents attached to the chro-
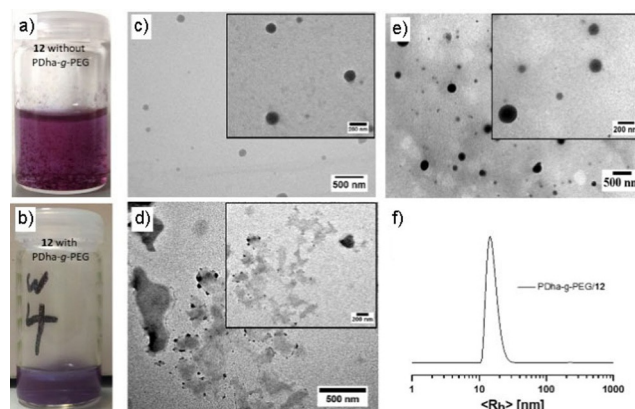
Figure 6. Compound **12** in aqueous solution a) without and b) with PDha-*g*-PEG. TEM micrographs of c) PDha-*g*-PEG/**12**, d) PDha-*g*-PEG/$[Mo_3S_{13}^{2-}]$, and e) PDha-*g*-PEG/$[Mo_3S_{13}^{2-}]$/**12**. f) DLS plot for PDha-*g*-PEG/**12**. (For DLS plots for PDha-*g*-PEG/$[Mo_3S_{13}^{2-}]$ and PDha-*g*-PEG/$[Mo_3S_{13}^{2-}]$/**12**, see Figure S26).
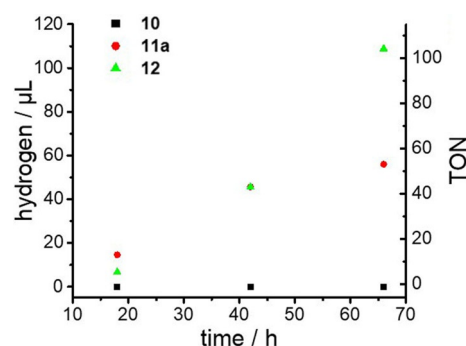
Figure 7. Photocatalytic hydrogen production of $[Mo_3S_{13}]^{2-}$ [21.5 μM] with **10**, **11a**, **12** [0.2 mM] in aqueous solution with PDha-*g*-PEG [0.13 mg mL⁻¹], ascorbic acid [2.5 mM] (pH 4). A detailed description is given in the Supporting Information.

Table 3. Redox potentials of catalyst, sacrificial electron donor and the photosensitizers [vs. Fc/Fc⁺].

	$[Mo_3S_{13}]^{2-}$	AA[54] [b]	**10**	**11a**	**12**
E_{ox1} [V]	–	0.08	0.59	0.53	0.57
E_{red1} [V]	−1.20	–	−1.40	−1.38	−1.40

[a] Onset potential in DMF. [b] In aqueous solution given vs. SCE, calculated to Fc/Fc⁺ by subtraction of 0.38 V.[53] [c] in CH_2Cl_2.

mophore, catalytic activity decreased from 1.1 h⁻¹ (TOF) in the first two days to 0.44 h⁻¹ during the third day. With its selenium analogue, high activity was still observed even after 3 days (2.6 h⁻¹). In contrast, **10** as photosensitizer did not result in any hydrogen production. Compound **10** does not have a long-lived excited state, so that luminescent relaxation stands in competition with intermolecular charge transfer. An estimation of the driving force for the possible electron transfer processes suggests a mechanism involving oxidative quenching by electron transfer from the excited photosensitizer to $[Mo_3S_{13}]^{2-}$ followed by re-reduction of the sensitizer by the sacrificial agent (Figure 8, estimation in the Supporting Information).

Chemistry–A European Journal

| Full Paper
doi.org/10.1002/chem.202004326

**Chemistry
Europe**
European Chemical
Societies Publishing

Figure 8. Proposed electron-transfer mechanism with reductive (blue arrow) and oxidative (red arrow) quenching. The energy level of the triplet state was obtained from phosphorescence measurements; the driving force was calculated from the Rehm–Weller equation (see the Supporting Information for both).

Conclusions

In summary, the synthetic approach of decarboxylative bromination was successfully applied to dibromo PDAs giving facile access to tetrabromo PMAs. Isomerically pure 1,7,9,10-tetrabromo **3a** and 1,6,9,10-tetrabromo **3b** perylene dibutyl esters were obtained upon esterification. X-ray diffraction analysis of the chromophores revealed a ball-shaped overlap of both the substituents and the distorted perylene framework for the tetrasubstituted diesters **5a** and **6**, while the packing behavior for **4** was found to be squared. Time-resolved spectroscopy showed the presence of a non-emissive long-lived excited state for **11a**, **11b** and **12** in contrast to **10**. In photocatalytic experiments, we proved that tetrasubstituted perylene monoimides **11a** and **12** are well suited for visible light sensitization of $[Mo_3S_{13}]^{2-}$ for proton reduction in the presence of a polymeric solubilizing agent. It is noteworthy, that the setup showed high catalytic durability, in particular for compound **12**, with a maximum TON of 104 after 3 days of irradiation. The chromophores presented here can be further modified for covalent integration within soft matter matrices or coupling to molecular proton reduction catalysts. This work provides a facile and ecofriendly synthetic route for fourfold brominated perylene diesters that can broaden the scope of potential photosensitizers by applying other nucleophiles, palladium-catalyzed cross-coupling and selective substitution of one, two or three bromo substituents.

Deposition numbers 2033579 (for **3a**), 2033580 (for **3b**), 2033581 (for **4**), 2033582 for (**5a**), and C2033583 (for **6**) contain the supplementary crystallographic data for this paper. These data are provided free of charge by the joint Cambridge Crystallographic Data Centre and Fachinformationszentrum Karlsruhe Access Structures service www.ccdc.cam.ac.uk/structures.

Conflict of Interests

The authors declare no conflict of interests.

[1] L. Yao, A. Rahmanudin, N. Guijarro, K. Sivula, *Adv. Energy Mater.* **2018**, *8*, 1802585.
[2] F. Würthner, *Chem. Commun.* **2004**, 1564–1579.
[3] J. Warnan, J. Willkomm, Y. Farre, Y. Pellegrin, M. Boujtita, F. Odobel, E. Reisner, *Chem. Sci.* **2019**, *10*, 2758–2766.
[4] C. Li, H. Wonneberger, *Adv. Mater.* **2012**, *24*, 613–636.
[5] G. Li, W. Yang, S. Wang, T. Liu, C. Yan, G. Li, Y. Zhang, D. Li, X. Wang, P. Hao, J. Li, L. Huo, H. Yan, B. Tang, *J. Mater. Chem. C* **2019**, *7*, 10901–10907.
[6] Z. Liu, D. Zeng, X. Gao, P. Li, Q. Zhang, X. Peng, *Sol. Energy Mater. Sol. Cells* **2019**, *189*, 103–117.
[7] J. Warnan, J. Gardner, L. Le Pleux, J. Petersson, Y. Pellegrin, E. Blart, L. Hammarström, F. Odobel, *J. Phys. Chem. C* **2013**, *117*, 8652.
[8] L. Le Pleux, A. L. Smeigh, E. Gibson, Y. Pellegrin, E. Blart, G. Boschloo, A. Hagfeldt, L. Hammarström, F. Odobel, *Energy Environ. Sci.* **2011**, *4*, 2075–2084.
[9] W. Liu, R. Tkachov, H. Komber, V. Senkovskyy, M. Schubert, Z. Wei, A. Facchetti, D. Neher, A. Kiriy, *Polym. Chem.* **2014**, *5*, 3404–3411.
[10] R. E. Cook, B. T. Phelan, L. E. Shoer, M. B. Majewski, M. R. Wasielewski, *Inorg. Chem.* **2016**, *55*, 12281–12289.
[11] R. J. Lindquist, B. T. Phelan, A. Reynal, E. A. Margulies, L. E. Shoer, J. R. Durrant, M. R. Wasielewski, *J. Mater. Chem. A* **2016**, *4*, 2880–2893.
[12] A. S. Weingarten, R. V. Kazantsev, L. C. Palmer, M. McClendon, A. R. Koltonow, A. P. Samuel, D. J. Kiebala, M. R. Wasielewski, S. I. Stupp, *Nat. Chem.* **2014**, *6*, 964–970.
[13] R. J. Kamire, M. B. Majewski, W. L. Hoffeditz, B. T. Phelan, O. K. Farha, J. T. Hupp, M. R. Wasielewski, *Chem. Sci.* **2017**, *8*, 541–549.
[14] I. T. G. Ghosh, J. I. Bardagi, B. König, *Science* **2014**, *346*, 725–728.
[15] M. Bonchio, Z. Syrgiannis, M. Burian, N. Marino, E. Pizzolato, K. Dirian, F. Rigodanza, G. A. Volpato, G. La Ganga, N. Demitri, S. Berardi, H. Amenitsch, D. M. Guldi, S. Caramori, C. A. Bignozzi, A. Sartorel, M. Prato, *Nat. Chem.* **2019**, *11*, 146–153.
[16] J. T. Kirner, R. G. Finke, *J. Mater. Chem. A* **2017**, *5*, 19560–19592.
[17] R. K. Gupta, A. Dey, A. Singh, P. K. Iyer, A. A. Sudhakar, *ACS Appl. Electron. Mater.* **2019**, *1*, 1378–1386.
[18] M. Kucinska, I. Frac, J. Ulanski, T. Makowski, A. Nosal, M. Gazicki-Lipman, *Synth. Met.* **2019**, *250*, 12–19.
[19] W. Rekab, M. A. Stoeckel, M. El Gemayel, M. Gobbi, E. Orgiu, P. Samori, *ACS Appl. Mater. Interfaces* **2016**, *8*, 9829–9838.
[20] S. Kaloyanova, Y. Zagranyarski, S. Ritz, M. Hanulová, K. Koynov, A. Vonderheit, K. Müllen, K. Peneva, *J. Am. Chem. Soc.* **2016**, *138*, 2881–2884.
[21] Q. Li, X. Hao, J. Guo, X. K. Ren, S. Xia, W. Zhang, Y. Feng, *Macromol. Rapid Commun.* **2019**, *40*, 1800916.

[22] T. Weil, T. Vosch, J. Hofkens, K. Peneva, K. Mullen, *Angew. Chem. Int. Ed.* **2010**, *49*, 9068–9093; *Angew. Chem.* **2010**, *122*, 9252–9278.

[23] K. Huth, M. Glaeske, K. Achazi, G. Gordeev, S. Kumar, R. Arenal, S. K. Sharma, M. Adeli, A. Setaro, S. Reich, R. Haag, *Small* **2018**, *14*, 1800796.

[24] T. Heek, C. Kuhne, H. Depner, K. Achazi, J. Dernedde, R. Haag, *Bioconjugate Chem.* **2016**, *27*, 727–736.

[25] A. Godoy, L. Cattin, J. C. Bernède, F. Díaz, M. A. del Valle, *Macromol. Symp.* **2011**, *304*, 109–114.

[26] V. Strauss, J. T. Margraf, C. Dirian, Z. Syrgiannis, M. Prato, C. Wessendorf, A. Hirsch, T. Clark, D. M. Guldi, *Angew. Chem. Int. Ed.* **2015**, *54*, 8292–8297; *Angew. Chem.* **2015**, *127*, 8410–8415.

[27] C. Li, J. Schoneboom, Z. Liu, N. G. Pschirer, P. Erk, A. Herrmann, K. Mullen, *Chem. Eur. J.* **2009**, *15*, 878–884.

[28] C. Li, J. H. Yum, S. J. Moon, A. Herrmann, F. Eickemeyer, N. G. Pschirer, P. Erk, J. Schoneboom, K. Mullen, M. Gratzel, M. K. Nazeeruddin, *ChemSusChem* **2008**, *1*, 615–618.

[29] R. K. Dubey, S. J. Eustace, J. S. van Mullem, E. J. R. Sudholter, F. C. Grozema, W. F. Jager, *J. Org. Chem.* **2019**, *84*, 9532–9547.

[30] J. Vollbrecht, H. Bock, C. Wiebeler, S. Schumacher, H. Kitzerow, *Chem. Eur. J.* **2014**, *20*, 12026–12031.

[31] A. G. Phillips, L. M. Perdigao, P. H. Beton, N. R. Champness, *Chem. Commun.* **2010**, *46*, 2775–2777.

[32] M. Franceschin, A. Alvino, G. Ortaggi, A. Bianco, *Tetrahedron Lett.* **2004**, *45*, 9015–9020.

[33] K. Zaugg, J. Velasco, K. A. Robins, D.-C. Lee, *ACS Omega* **2019**, *4*, 5434–5441.

[34] Y. H. I. Shibano, C. Adachi, *J. Phys. Chem. C* **2009**, *113*, 15454–15466.

[35] Y. Zhao, X. Li, Z. Wang, W. Yang, K. Chen, J. Zhao, G. G. Gurzadyan, *J. Phys. Chem. C* **2018**, *122*, 3756–3772.

[36] A. Keerthi, Y. Liu, Q. Wang, S. Valiyaveettil, *Chem. Eur. J.* **2012**, *18*, 11669–11676.

[37] D. Sahoo, V. Sharma, R. Roy, N. Varghese, K. Mohanta, A. L. Koner, *Chem. Commun.* **2018**, *54*, 12883.

[38] V. Sharma, K. Kovida, D. Sahoo, N. Varghese, K. Mohanta, A. L. Koner, *RSC Adv.* **2019**, *9*, 30448–30452.

[39] Y. L. C. Zagranyarski, Y. Zhao, H. Wonneberger, C. Li, K. Müllen, *Org. Lett.* **2012**, *14*, 5444–5447.

[40] D. Jänsch, I. Ivanov, Y. Zagranyarski, I. Duznovic, M. Baumgarten, D. Turchinovich, C. Li, M. Bonn, K. Mullen, *Chem. Eur. J.* **2017**, *23*, 4870–4875.

[41] H. Abul-Futouh, A. Skabeev, D. Botteri, Y. Zagranyarski, H. Görls, W. Weigand, K. Peneva, *Organometallics* **2018**, *37*, 3278–3285.

[42] S. Sengupta, R. K. Dubey, R. W. Hoek, S. P. van Eeden, D. D. Gunbas, F. C. Grozema, E. J. Sudholter, W. F. Jager, *J. Org. Chem.* **2014**, *79*, 6655–6662.

[43] F. V. S. Würthner, Z. Chen, C. R. Saha-Möller, N. Kocher, D. Stalke, *J. Org. Chem.* **2004**, *69*, 7933–7939.

[44] Y. Zagranyarski, L. Chen, D. Jansch, T. Gessner, C. Li, K. Müllen, *Org. Lett.* **2014**, *16*, 2814–2817.

[45] C. Janiak, *J. Chem. Soc. Dalton Trans.* **2000**, *21*, 3885–3896.

[46] N. J. Hestand, R. V. Kazantsev, A. S. Weingarten, L. C. Palmer, S. I. Stupp, F. C. Spano, *J. Am. Chem. Soc.* **2016**, *138*, 11762–11774.

[47] B. Harutyunyan, A. Dannenhoffer, S. Kewalramani, T. Aytun, D. J. Fairfield, S. I. Stupp, M. J. Bedzyk, *J. Phys. Chem. C* **2017**, *121*, 1047–1054.

[48] R. V. Kazantsev, A. J. Dannenhoffer, A. S. Weingarten, B. T. Phelan, B. Harutyunyan, T. Aytun, A. Narayanan, D. J. Fairfield, J. Boekhoven, H. Sai, A. Senesi, P. I. O'Dogherty, L. C. Palmer, M. J. Bedzyk, M. R. Wasielewski, S. I. Stupp, *J. Am. Chem. Soc.* **2017**, *139*, 6120–6127.

[49] A. Nowak-Król, F. Würthner, *Org. Chem. Front.* **2019**, *6*, 1272–1318.

[50] Y. Zhao, R. Duan, J. Zhao, C. Li, *Chem. Commun.* **2018**, *54*, 12329–12332.

[51] Y. Zhao, A. A. Sukhanov, R. Duan, A. Elmali, Y. Hou, J. Zhao, G. G. Gurzadyan, A. Karatay, V. K. Voronkova, C. Li, *J. Phys. Chem. C* **2019**, *123*, 18270–18282.

[52] X. Zhang, A. Elmali, R. Duan, Q. Liu, W. Ji, J. Zhao, C. Li, A. Karatay, *Phys. Chem. Chem. Phys.* **2020**, *22*, 6376–6390.

[53] V. V Pavlishchuk, A. W Addison, *Inorg. Chim. Acta* **2000**, *298*, 97–102.

[54] Y. Pellegrin, F. Odobel, *C. R. Chim.* **2017**, *20*, 283–295.

[55] A. Vlček, *Coord. Chem. Rev.* **2000**, *200–202*, 933–977.

[56] M. Dave, A. Rajagopal, M. Damm-Ruttensperger, B. Schwarz, F. Nägele, L. Daccache, D. Fantauzzi, T. Jacob, C. Streb, *Sustainable Energy Fuels* **2018**, *2*, 1020–1026.

[57] M.-L. Grutza, A. Rajagopal, C. Streb, P. Kurz, *Sustainable Energy Fuels* **2018**, *2*, 1893–1904.

[58] K. A. Click, D. R. Beauchamp, Z. Huang, W. Chen, Y. Wu, *J. Am. Chem. Soc.* **2016**, *138*, 1174–1179.

[59] A. S. Weingarten, A. J. Dannenhoffer, R. V. Kazantsev, H. Sai, D. Huang, S. I. Stupp, *J. Am. Chem. Soc.* **2018**, *140*, 4965–4968.

[60] J. Kibsgaard, T. F. Jaramillo, F. Besenbacher, *Nat. Chem.* **2014**, *6*, 248–253.

[61] J. B. Max, D. V. Pergushov, L. V. Sigolaeva, F. H. Schacher, *Polym. Chem.* **2019**, *10*, 3006–3019.

[62] J. B. Max, K. Kowalczuk, M. Köhler, C. Neumann, F. Pielenz, L. V. Sigolaeva, D. V. Pergushov, A. Turchanin, F. Langenhorst, F. H. Schacher, *Macromolecules* **2020**, *53*, 4511–4523.